Journal of Quantitative Spectroscopy & Radiative Transfer 331 (2025) 109252

Contents lists available at ScienceDirect

Journal of Quantitative Spectroscopy and Radiative Transfer

journal homepage: www.elsevier.com/locate/jqsrt

Update Granada–Amsterdam Light Scattering Database

O. Muñoz [a,*], E. Frattin [a], J. Martikainen [a], D. Guirado [a], M. Passas-Varo [a], J. Escobar-Cerezo [a,f], F.J. García-Izquierdo [a], J.C. Gómez-Martín [a], Z. Gray [b,c,d], T. Jardiel [e], F. Moreno [a], A.J. Ocaña [a], M. Peiteado [e], A.T. Gallego-Calvente [a,h], H. Volten [g]

[a] Instituto de Astrofísica de Andalucía, CSIC, Glorieta de la Astronomía sn, Granada, 18008, Spain
[b] Mullard Space Science Laboratory, University College London, Holmbury St. Mary, Dorking, London, RH5 6NTN, UK
[c] Armagh Observatory and Planetarium, College Hill, Armagh, BT61 9DGR, Northern Ireland, UK
[d] The Centre for Planetary Sciences, UCL/Birkbeck, London, WC1E 6BT, UK
[e] Instituto de Cerámica y Vidrio, CSIC, Kelsen 5, Campus Cantoblanco, Madrid, E-28049, Spain
[f] Hospital Universitario Clínico Virgen de las Nieves, Avda. del Conocimiento s/n, Granada, 18014, Spain
[g] Netherlands National Institute for Public Health and the Environment, Centre for Environmental Monitoring, P.O. Box 1, Bilthoven, NL 3720 BA, The Netherlands
[h] Departament d Astronomia i Astrofísica. Universitat de Valencia, Doctor Moliner, 50, Burjassot, Valencia, E-46100, Spain

ARTICLE INFO

Keywords:
Scattering matrix
Experiments
Irregular particles
Polarization

ABSTRACT

We present an update to the Granada–Amsterdam Light Scattering Database (https://scattering.iaa.es/), which includes experimental data from both the IAA-Cosmic Dust Laboratory in Granada and the Amsterdam light scattering setup. The updated version features an expanded collection of samples and a more user-friendly interface. We have extended the size range of our mineral samples to mm-cm-sized single particles. Additionally, we have added the diffuse reflectance spectra of some of our powder samples and, from these spectra, obtained the corresponding refractive indices (200 nm–2000 nm). We have also incorporated synthetic scattering matrices defined across the entire scattering angle range (0° to 180°) for most of the powder samples contained in the database. Data in the database are freely available under the request of citation of this paper and the paper in which the data are published.

1. Introduction

Light scattering measurement data are scarce, not many instruments exist that produce reliable data. Even less of that data are available as open and FAIR (Findable, Accessible, Interoperable and Re-usable) data, with enough meta data to make them truly useful for comparison to light scattering model data, as input for atmospheric models, or satellite retrieval, to name a few of the applications the data may be used for. Yet properly documented and open light scattering measurement data are very durable and remain relevant for a long time. When the first hydrosol measurement performed at the Amsterdam light scattering setup were published in 1998 [1], people were still referring to volume scattering functions measured by [2]. These data by Petzold were published in a book about ocean water in the form of a table and were therefore extremely useful for the research community, even though being more than 20 years old. To stimulate the use of the data for further research, the first papers about the measurements performed with the Amsterdam light scattering setup tried to provide the same service. They contained a lot of tables with data and meta data such as size distributions.

When around the year 2000 the internet became more widely and easily accessible, the idea came up to build the Amsterdam light scattering database that contained measured light scattering matrices and the meta data describing scattering samples and information on how to interpret and use the data [3]. This meant giving other researchers access to data without exerting any influence on how the data would be used, or whether the work would be properly referenced or credited. But the benefits turned out to be large. Removing almost all barriers to the use of the experimental light scattering data caused a wide uptake of the data by modelers [4–11]. Feedback from the users of the data was then used to make improvements to the Amsterdam light scattering database such as the addition of the average scattering matrices and the synthetic scattering matrix with the full angle range included [12]. After the closing of the Dutch scattering apparatus, the database has been fed by the experimental data obtained at the IAA-Cosmic Dust Laboratory [13,14]. This resulted in the joint Amsterdam-Granada

* Corresponding author.
E-mail address: olga@iaa.es (O. Muñoz).
URL: https://scattering.iaa.es (O. Muñoz).

https://doi.org/10.1016/j.jqsrt.2024.109252
Received 12 July 2024; Received in revised form 18 October 2024; Accepted 28 October 2024
Available online 12 November 2024

Light Scattering database, which compiled the data produced by both laboratories [15]. It was structured so that from the homepage, users could access the data obtained in Amsterdam or the new data obtained in Granada. Open access to the experimental data has facilitated its utilization and application by a plethora of research groups e.g. [16–20].

In this day and age of open and FAIR data the database remains as relevant as ever. We describe here the new structure of the Granada–Amsterdam Light scattering database (GALSD) and the recent additions made. The paper is organized as follows: Section 2 provides a brief description of the IAA light scattering apparatus including a summary of the performance tests developed to assure that the scattering matrices included in the database correspond to randomly oriented particles under single-scattering conditions. Sections 3 and 4 describe the database structure and content, respectively. Section 5 presents the new additions to the database, while Section 6 provides an example of using the database through its application to characterizing cometary dust.

2. IAA Cosmic Dust Laboratory

The Cosmic Dust Laboratory (CODULAB) is located at the Instituto de Astrofísica de Andalucía in Granada, Spain. A comprehensive technical description of the scattering apparatus, data acquisition, and reduction process is provided by [13]. The experiment schematic block diagram, photograph, movie, tests measurements, and related papers are available on the "Experimental Apparatus" page of the database https://scattering.iaa.es/apparatus.

In brief, light from a diode laser (available wavelengths are 405, 488, 514 and 640 nm) passes through a polarizer and an electro-optic modulator and is scattered by the sample placed at the center of the set-up. By combining electro-optic modulation of the incident beam with lock-in detection, we enhance the accuracy of our measurements and simultaneously determine several elements of the 4 × 4 scattering matrix, **F** [21]:

$$\mathbf{F} = \begin{pmatrix} F_{11} & F_{12} & F_{13} & F_{14} \\ F_{21} & F_{22} & F_{23} & F_{24} \\ F_{31} & F_{32} & F_{33} & F_{34} \\ F_{41} & F_{42} & F_{43} & F_{44} \end{pmatrix}. \quad (1)$$

The scattered light is detected by two photomultipliers (detector and monitor). The detector moves along a ring covering scattering angles between 3° to 177°, while the monitor is placed at a fixed angular position and serves to control the fluctuations of the laser signal and/or dust jet stream from the aerosol generator. There are two optional optical elements in front of the detector (a quarter waveplate and an analyzer). The elements F_{ij} of the scattering matrix are dimensionless and depend on the physical properties of the particles (morphology, size, and refractive index), the wavelength of the incident beam, and the direction of scattering. The direction of scattering is defined by the angle between the propagation directions of the incident and scattered beams, i.e., the scattering angle, θ, ranging from 0 to π, and an azimuth angle Φ that ranges from 0 to 2π. For randomly oriented particles, as is the case in our experiment, all scattering planes are equivalent, and the scattering direction is fully described by the scattering angle. Further, in case the cloud contains a sufficient number of particles so that mirror symmetry in the ensemble can be assumed, the 4 × 4 scattering matrix, for each scattering angle, is defined as (see e.g. [22]).

$$F = \begin{pmatrix} F_{11} & F_{12} & 0 & 0 \\ F_{12} & F_{22} & 0 & 0 \\ 0 & 0 & F_{33} & F_{34} \\ 0 & 0 & F_{43} & F_{44} \end{pmatrix} \quad (2)$$

The cloud of randomly oriented μm-sized particles is produced by an aerosol generator as follows: a compacted amount of powder is loaded into a cylindrical reservoir. A piston pushes the powder onto a rotating brush at a certain speed, adjustable from 0 to 400 mm/h. An air stream carries the aerosol particles from the brush through a tube to a nozzle above the scattering volume. Fig. 1 displays the aerosol generator dispersion unit.

2.1. Testing the performance of the scattering apparatus

The performance of the scattering apparatus is evaluated by comparing the measured scattering matrix elements of a selected set of well-characterized spherical particles (in terms of size, sphericity, and refractive index) with the results from Lorenz–Mie calculations for the corresponding size and refractive index. This applies to clouds of spherical micron-sized water droplets produced by a nebulizer [13] or a single well-characterized sphere [23]. For the latter, we have chosen a N-BK7 glass sphere (Edmund Optics) with a radius similar to that of the dust grain of interest. Fig. 2 shows an example of test measurements with water droplets. It displays the measured and computed scattering matrix of spherical water droplets at 520 nm. We do not show the ratios $F_{13}(\theta)/F_{11}(\theta)$, $F_{14}(\theta)/F_{11}(\theta)$, $F_{23}(\theta)/F_{11}(\theta)$, and $F_{24}(\theta)/F_{11}(\theta)$ since we verified that they are equal to zero within the error bars at the full measured scattering angle range. As described in [13], for the Lorenz–Mie calculations, we assume a two parameters (r_g, σ_g) log-normal size distribution as defined by [24]. In the fitting procedure, the water droplets refractive index is fixed to $m = 1.33 + 0.0i$. The parameters for the size distribution are selected to minimize the differences between the measured and calculated values of $F_{11}(\theta)$ and $-F_{12}(\theta)/F_{11}(\theta)$. As shown, the water droplets measurements show an excellent agreement with the Lorenz–Mie computations over the entire angle range. These test measurements assure the reliability of further measurements with irregular particles.

2.2. Single-scattering test

After testing the optical train alignment and optimum control parameter for our apparatus electronic devices, we must check that our measurements are performed under single scattering conditions. During the measurements, we need a sufficient number of particles in the scattering volume to represent an ensemble of randomly oriented particles of diverse sizes and shapes, while ensuring that the particle density is low enough to minimize the impact of multiple scattering. To test that this is the case, we follow the procedure described by [22]. With the detector fixed in position, a series of measurements are conducted with increasing sample concentrations. Multiple scattering is considered negligible as long as the scattered flux remains proportional to the aerosol concentration. This method aids in determining the optimal sample concentration. During a typical light scattering measurement using a dust sample, the speed of the aerosol generator piston (Fig. 1) needs to be sufficiently high to maintain a stable aerosol stream, yet not excessively high to prevent unnecessary sample wastage. Typically, the piston speed ranges from 40 to 100 mm/h, depending on the specific sample under study. As shown in Fig. 3, in the single scattering test the piston speed was adjusted from 50 mm/h to 250 mm/h in increments of 50 mm/h. Even at speeds as high as 250 mm/h, we observed no significant departure from a linear behavior [14,22], indicating that multiple scattering effects can be disregarded in our experiments.

2.3. Particle random orientation test

The scattering matrix definition as presented in Eq. (2) assumes that the particles in the scattering volume are randomly oriented. As shown in Fig. 1, the aerosol generator's nozzle is positioned directly above the scattering volume, causing the aerosol jet to flow perpendicularly through it. This setup suggests that the particles within the scattering volume do not exhibit a specific orientation, except for a potential orientation in the direction of the jet stream. However, we have verified that there is not preferential alignment along the aerosol

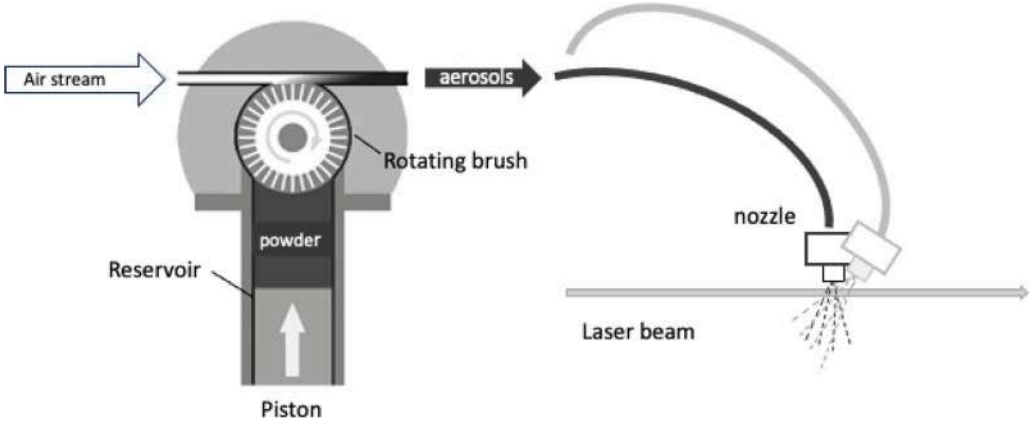

Fig. 1. Schematic picture of the aerosol generator (RBG 1000 Palas) dispersion unit. The piston pushes powder onto the rotating brush at a certain speed expressed in mm/h. An air stream carries the aerosol particles of the brush through a tube to a nozzle right above the scattering volume. The aerosol jet is directed perpendicular to the scattering plane (black nozzle). Gray nozzle shows the setup during the random orientation test.

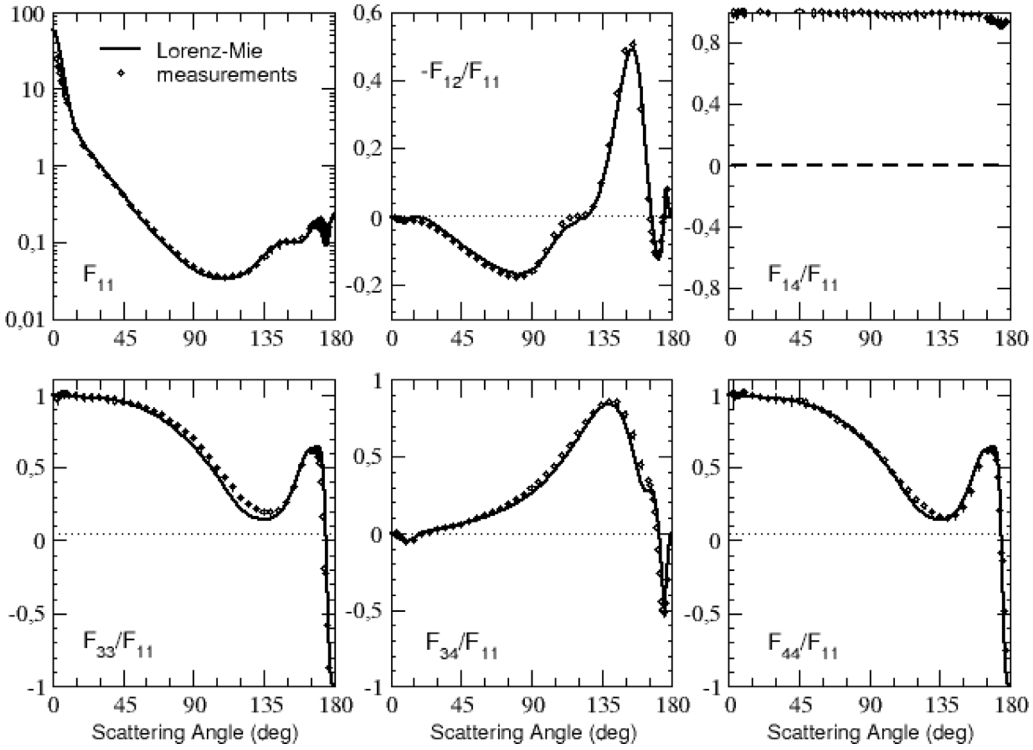

Fig. 2. Comparison of simulated and measured scattering matrices for water droplets at 520 nm. The measurements are indicated with circles and error bars. Solid lines correspond to results of Lorenz–Mie computations at 520 nm for a log-normal size distribution (r_g = 0.8 μm, σ = 1.5). Measured and computed data for the F_{11} element are normalized to 1 at 30 degrees.

beam either. To achieve this, the aerosol nozzle was positioned at a 45-degree angle to the scattering plane (gray nozzle in Fig. 1). We conducted scattering matrix measurements for a clay sample at 632.8 nm and found no significant differences in the elements of the scattering matrix as functions of the scattering angle for the two orientations of the particle jet [22]. Therefore, the orientation of the particle jet stream does not significantly impact our experimental results, and the particles in our experiments can be considered randomly oriented. Further, measuring all elements of the scattering matrix provides extra random-orientation, reciprocity, and mirror symmetry tests (https://scattering.iaa.es/matrix, [25]). For instance, the measured elements of the scattering matrix fulfill the theoretical relations $F_{13}(\theta)/F_{11}(\theta) \equiv F_{14}(\theta)/F_{11}(\theta) \equiv F_{23}(\theta)/F_{11}(\theta) \equiv F_{24}(\theta)/F_{11}(\theta) \equiv 0$, which hold for an ensemble of randomly oriented particles with equal numbers of mirror particles. Since these elements are zero at all scattering angles for all our measured powders so far, we typically omit these scattering matrix elements from figures.

3. Database structure

In this section, we describe the information provided by the database from a user's point of view. The home page of the database is depicted in Fig. 4. The main website leads to 6 pages, namely : list of all samples, sample categories, news, papers, theory, and experimental apparatus.

- **List of all Samples:** This page lists all samples included in the database organized in five different categories: Aerosols (clouds of micron-sized particles), hydrosols, mm-sized single particles, average scattering matrices, and test particles. In this way, the user can check if the sample of interest is included in the database

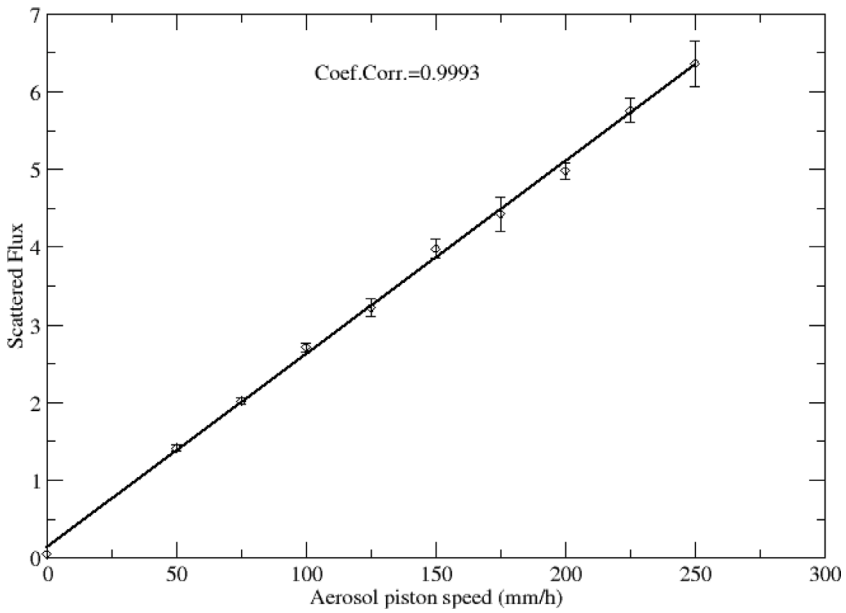

Fig. 3. Scattered flux (in arbitrary units) at $\theta = 10°$ versus aerosol generator piston speed for white clay particles. After [14].

Fig. 4. Home page of the Granada–Amsterdam Light Scattering Database, available at https://scattering.iaa.es/.

without the need to dive through it. Within each category, the samples are organized in alphabetical order including information on their size/size distribution, wavelength(s), and scattering-angle range at which the measurements have been performed. Further, for some samples the database provides the retrieved sample refractive index in the wavelength range from 200 to 2000 nm. Details on the refractive index retrieval procedure are provided in Section 5.1.

- **Sample Categories:** This page consists of six sub-categories, namely: micron-cosmic analogs, mm-cosmic analogs, terrestrial aerosols, meteorites, hydrosols, and Martian analogs (Fig. 5). The content of each category is described in detail in Section 4.
- **News:** The news page is continuously updated with new published papers that imply new data in the database or general information on light scattering as is the case of related conference or topical journal issues.
- **Papers:** It displays all papers linked to the database in alphabetical order. All measurements presented in the database have been previously published in peer-reviewed scientific journals. The data in the database are freely available under request of citation of this paper and the paper in which the experimental data are published.
- **Theory:** The primary objective of this page is to clarify the meaning of the data provided in the database, thereby aiding in the proper utilization of the experimental data. It comprises the following pages: Stokes vector & Scattering matrix; What do we measure?; Synthetic Matrix, Size Distribution, Particle composition & Refractive indices; and SEM images. The Particle composition & Refractive indices and Synthetic Matrix are discussed in Sections 5.1 and 5.4, respectively.
- **Experimental Apparatus:** This page includes a schematic overview of the IAA light scattering apparatus along with a photograph and a short movie. As mentioned, the performance of the scattering setup is tested by direct comparison of the experimental scattering matrices of spherical particles to results of Lorenz–Mie computations. This page provides the measured scattering

Fig. 5. Sample categories page of the Granada–Amsterdam Light Scattering Database.

matrices for test particles at different wavelengths. Detailed information on the light scattering apparatus and data reduction process is also provided in [13,14].

4. Database contents

The core of the database includes tables and figures of the measured scattering matrix elements as functions of the scattering angle at various wavelengths. Additionally, it provides detailed characterization of the samples, including size/size distributions tables and figures, composition, origin, optical and/or scanning electron microscope images, and information on the refractive indices of the particles based on literature values. By clicking at the sample name either from the "list of samples" or "sample categories" pages, the user has access to the corresponding fact sheet that includes tables and figures. Recently, we have added the diffuse reflectance spectra of the powders (200 to 2000 nm) to the database. From the reflectance spectra, we derive the complex refractive indices (see Section 5.1). All papers in pdf format, full references, and citations in BibTeX format are also provided.

4.1. Samples

The particle samples included in the database comprise a wide range in origin, size and composition. The "List of samples" page displays all samples organized in five categories: Aerosols, Hydrosols, mm-sized grains, Average scattering matrices and Test measurements. The samples included in each category are described below.

4.1.1. Aerosols

The aerosols-category encompasses all samples composed of clouds of powders in random orientation. As detailed in Section 2, these clouds are produced by an aerosol generator. The aerosol samples include particles with radii ranging from sub-micron to 100 micrometers. To enhance the accessibility and usability of the Granada–Amsterdam data collection, the aerosol samples have been divided into four subcategories based on their potential applications: micron-cosmic analogs, terrestrial aerosols, meteorites, and Martian analogs. We note that some samples might be included in various categories. Those are the cases of the meteorites and Martian analogs that are subsets of the micron-cosmic analogs category.

4.1.2. Hydrosols

The hydrosols collection comprises the F_{11} and $-F_{12}/F_{11}$ curves for 15 different types of coastal and inland water phytoplankton species and two types of estuarine sediments [1]. The hydrosols measurements were performed at the Amsterdam light scattering setup [25,26]. The hydrosol sample is contained in a cylindrically shaped cuvette (d = 30 mm) of pyrex glass. The cuvette is located in the center of a 22 cm (diameter) basin filled with glycerine. Glycerine and glass have the same refractive index (m = 1.5) at the measured wavelength (632.8 nm). In this way, the reflexions produced by the strong change in refractive index air–glass occur farther away from the scattering volume. The measured scattering-angle range with the hydrosols setup is constrained to 25–155 degrees.

4.1.3. mm-sized single grains

The range of particles sizes included in the GALSD has been recently extended up-to the millimeter size range [23,27]. The millimeter-sized regime is particularly significant in protoplanetary disks [28], cometary dust tails [29], or asteroidal regolith [30]. For those measurements, the particle/grain is positioned on a conical-tip black holder, which is mounted on an x–y rotating table. Further, a beam expander is necessary to uniformly illuminate the entire cross-section of the sample. Further details on the procedure to simulating random orientation are provided in Section 5.2.

4.1.4. Average scattering matrices

The first dataset for mineral samples obtained in Amsterdam in the late 1990s demonstrated that the measured scattering matrix elements for different samples fell within relatively narrow ranges when plotted against the scattering angle. This similarity justified the creation of an initial Average Scattering Matrix for mineral aerosols by combining experimental data at 441.6 nm and 632.8 nm [26]. Further measurements of terrestrial aerosols demonstrated that grouping the non-zero scattering matrix elements of samples with a common origin, such as volcanic ash or desert dust, led to even tighter clustering when plotted against the scattering angle. This led us to construct separate Average Scattering Matrices for volcanic ashes and desert dust, which can be used for remote sensing studies when specific aerosol properties are unknown. The Average Scattering Matrix for volcanic ashes is available at blue (combined data at 441.6 nm and 488 nm) and red (combined data at 632.8 nm and 647 nm) wavelengths. It is derived from the measured scattering matrices for 11 samples of volcanic ashes:

Pinatubo, Lokon, Redoubt A, Redoubt B, Spurr Gunsight, Spurr Stop 33, Spurr Anchorage, Mt. St. Helens, El Chichón, Puyehue, and Eyjafjallajökull [26,31–33]. For desert dust, the average scattering matrices are available at 448 and 647 nm, derived from the scattering matrices for two airborne desert dust samples: Gobi and Sahara-OSN [33]. Details on the average scattering matrices construction are provided in [32].

4.1.5. Test samples

In accordance to the FAIR principles recommended by the European Commission, apart from detailed information on the experimental procedure we also provide tables with the test measurements with spherical water droplets and glass spheres. They are available via the list of samples and the Experimental Apparatus pages.

4.2. Powder size distributions

In the database we provide tables of the normalized number, n(r), projected-surface-area, s(r), and volume, v(r), and corresponding N(logr), S(logr) and V(logr) particle size distributions of the powder samples. Definitions and interrelations for these size distribution are available in the database at https://scattering.iaa.es/size. As example, Fig. 6 displays the measured size distributions for a sample consisting of a forsterite powder [34]. Values for the corresponding effective radius and variances as defined by [24] are also provided in the database.

The projected-surface-area size distributions of the samples studied in Amsterdam were measured using a Fritsch laser particle sizer [35], which employs Fraunhofer diffraction theory for spheres. The particle sizer used in Granada is a Mastersizer 2000 from Malvern Instruments. The Matersizer retrieval is obtained by using either the Lorenz–Mie theory or the Fraunhofer approximation for spheres. A detailed study of the range of validity of the Laser light scattering particle sizer can be found in [36] and https://scattering.iaa.es/size. Briefly:

For spherical particles at visible wavelengths (λ = 633 or 466 nm):

- In the case of highly absorbing particles, the Fraunhofer retrieval can be safely applied for particles radii, r > 0.5 μm. In any other case the lower limit is increased up to r > 3 μm (λ = 633 nm). This limit is reduced by a factor of ∼0.7 if the measurements are carried out at 466 nm.
- The Mie model with the correct refractive index constrains the intrinsic applicability method to r > 0.1μm. Claims of sensitivity below this limit must be regarded with scepticism if additional supporting techniques (e.g. polarimetry) are not considered.

For irregular particles at visible wavelengths (λ = 633 or 466 nm):

- The limit of applicability of the Fraunhofer retrieval is lowered to r ∼ 1 μm (λ = 466 nm) even for transparent particles. Fraunhofer cannot be generally trusted below that limit.
- The retrieval based on the Mie theory extends the validity almost to the lower limit for spheres (r ∼ 0.3 μm) if the real part of the refractive index *(n)* is high. Note that if n is uncertain, it is safer to assume values at the upper end of the uncertainty limit.

5. What is new in the database?

5.1. Samples reflectance spectra and refractive indices (200–2000 nm)

The diffuse reflectance spectra of the samples are measured over the wavelength range of 200 to 2000 nm using a Varian Cary 5000 UV–vis–NIR spectrophotometer with a 'praying mantis' diffuse reflectance accessory. The instrument is equipped with a deuterium arc source for the UV wavelengths and a halogentungsten source for the vis–NIR region. The samples are deposited in a small bowl-shaped powder holder and gently compressed so that they present a flat surface to the incident light. Three measurements of each sample are performed and each spectrum is calibrated using a polytetrafluoroethylene (PTFE) reflectance standard. The final spectrum is obtained by averaging the three measurement sets of the individual samples. The refractive index retrieval is based on the method developed by [37,38]. The method utilizes the measured diffuse reflectance spectra and particle size distributions in geometric optics regime together with state-of-the art light-scattering codes that account for irregular particle shapes. Currently, we only provide complex refractive indices for a set of Martian dust analog samples. We plan to expand the retrieval to other samples in the database.

5.2. Single mm-cm sized particles in random orientation

As mentioned, the particle size range in the GALSD collection has been recently expanded up to the millimeter-sized range. Apart from the need to adapt the optical setup (Section 4.1.3), it also involves a dedicated measurement procedure: The $F_{i,j}(\theta)$ in random orientation is obtained by averaging over 54 $F^o_{i,j}(\theta)$ corresponding to 54 particle orientations. The holder is mounted on a x–y rotating table. First, the particle is placed on the holder as shown in Fig. 7 (I). Starting from this position, each $F^o_{i,j}(\theta)$ is measured after each of 36 successive rotations of 10 degrees around the vertical axis (Z). Second, as shown in Fig. 7 (II), the particle is rotated 90 degrees towards the direction of the laser. From this position, the particle scattering pattern is measured in each of 18 successive rotations in steps of 20 degrees around the Z-axis. According to [39], a rigorous 3D orientation average can be achieved through a sufficient number of Euler rotations: (a) rotation around the vertical axis, (b) rotation around the x-axis, and (c) rotation around the axis perpendicular to the base of the particle. However, such a procedure requires a mechanical holder with two degrees of freedom and an excessive amount of experimental time. Instead, our procedure simplifies this rigorous approach by using only one rotation around the x-axis (90 degrees). The number of orientations used to simulate random orientation is in agreement with the estimates from [40] based on the experimental data at the microwave analog experiment located at the Fresnel institute [41] and numerical simulations.

There is still a range of particle sizes that cannot be studied with either the aerosol generator (radii from sub-micron up to 100 microns) or the previously described conical support (mm-cm sized). To address this gap and to facilitate random orientation measurements with large (r > 300 μm) single particles, we have developed an ultrasonic levitator that allows us to study grains with radii of a few hundred microns. The levitator is composed of 35 ultrasonic traducers operating at 40 kHz configured to form a spherical cavity. The force produced in the center of the cavity is sufficient for levitating spinning grains up to 50 mg of mass [42].

5.3. Narrow size distributions

The primary goal of our experimental work is to fill the existing gaps in our understanding of the interaction between electromagnetic radiation and non-spherical particles i.e. to disentangle the effects of size, composition, and shape on the scattering behavior of irregular particles. This requires the production of different sets of samples in which only one of the physical properties is varied. The first attempts [43,44] were devoted to study the size effect on the scattering pattern of clouds of magnesium-rich olivine (forsterite) samples. However, the milling/sieving procedures used to produce narrow size distributions from the bulk olivine samples were not efficient enough. This problem has been solved by applying processing routines from the fields of nano-, and micro-ceramics to synthesize well-defined narrow size distributions. The sample processing strategy combines different stages of milling, sieving, centrifuging and decanting, followed by several refining cycles in ultrasonic bath to remove small particles electrostatically attached to the surface of larger particles. Detailed description of the sample production process is provided by [34,38,45] along with

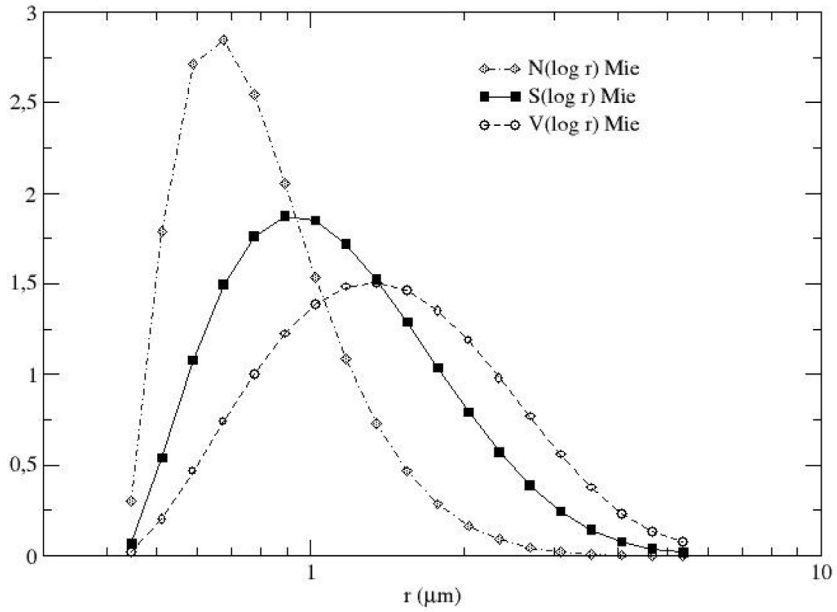

Fig. 6. Normalized number distribution N(logr), surface equivalent sphere distribution S (logr), and volume distribution V(logr) for Forsterite S sample described in [34].

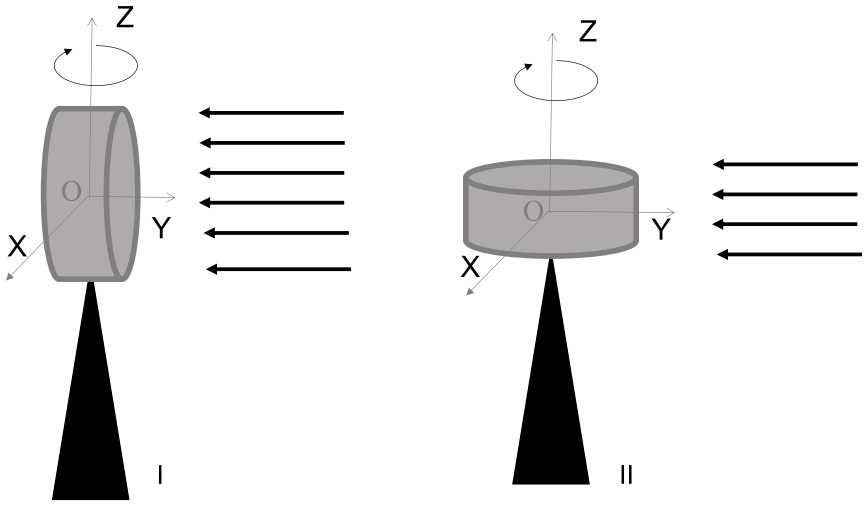

Fig. 7. (I) Particle initial position. (II) Particle after a 90 degrees rotation.
Source: Figure adapted from [23].

experimental scattering matrices for a set of forsterite and Martian analog samples, respectively. The particle size distributions span over a wide scattering size parameter domain: Rayleigh-resonance, resonance, and geometric optics. Although the data presented in [34,38,45] are focused on the characterization of cosmic dust and Martian aerosols, respectively, they may also be of interest for e.g. theoretical studies or the characterization of terrestrial aerosols. As an example, Fig. 8 displays the projected surface area distributions as function of radius (left panel) and measured $-F_{12}/F_{11}$ and F_{22}/F_{11} curves (right panel) for two forsterite samples. The corresponding effective radii and variances are also presented. As shown, both $-F_{12}/F_{11}$ and F_{22}/F_{11} curves show a strong dependence on particle size. Further, forsterite S shows anti-correlation between the $-F_{12}/F_{11}$ negative polarization branch and the F_{22}/F_{11} surge at backward direction. In the case of forsterite L, the negative polarization branch becomes shallower and the F_{22}/F_{11} shows no structure at backward direction. This link between the scattering mechanism responsible for the negative polarization branch and the behavior of the F_{22}/F_{11} at backward direction was previously suggested by [46,47] based on computed values for a set of irregular geometries with similar sizes as the forsterite S sample.

5.4. Synthetic scattering matrix

As mentioned, at CODULAB our measurable scattering angle range is restricted to [3, 177] degrees at best [14]. However, for various purposes, such as radiative transfer modeling, the full scattering angle range is often required (e.g. [48]). For those cases, an extrapolation of the measured scattering matrix during data processing can be performed by assuming certain necessary mathematical and physical conditions. A preliminary version of the extrapolation algorithm was presented by [32]. Since then, it has been subsequently revised and improved [33,49,50]. We refer to [51] for a comprehensive description of the extrapolation procedure. The so-called synthetic (extrapolated) scattering matrices are defined over the entire range from 0° to 180°. To facilitate the use of the experimental data in radiative transfer models, we have recently added tables with the synthetic scattering

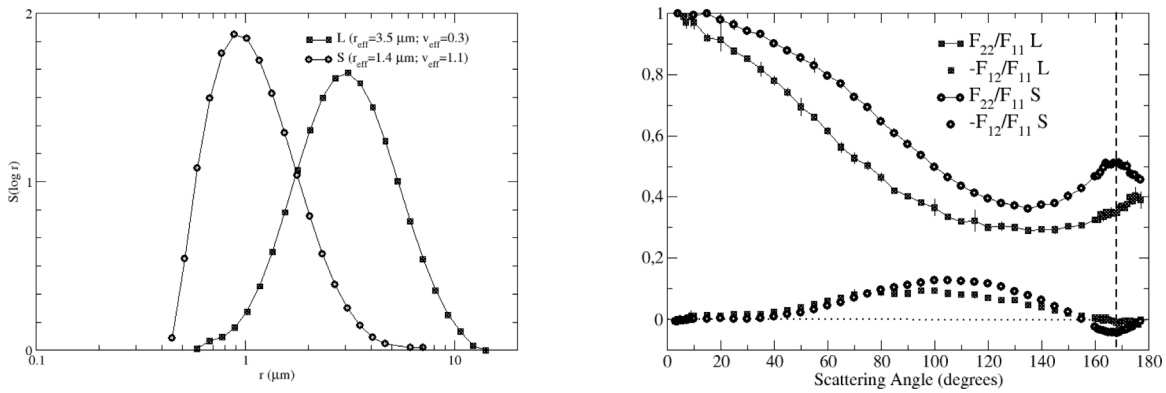

Fig. 8. Left: Projected surface area distribution as function of radius in micrometers in a logarithmic scale for forsterite L (squares) and S (circles). Right: Measured $-F_{12}/F_{11}$ and F_{22}/F_{11} curves for two forsterite samples: L (squares) and S (circles).
Source: Figure adapted from [34].

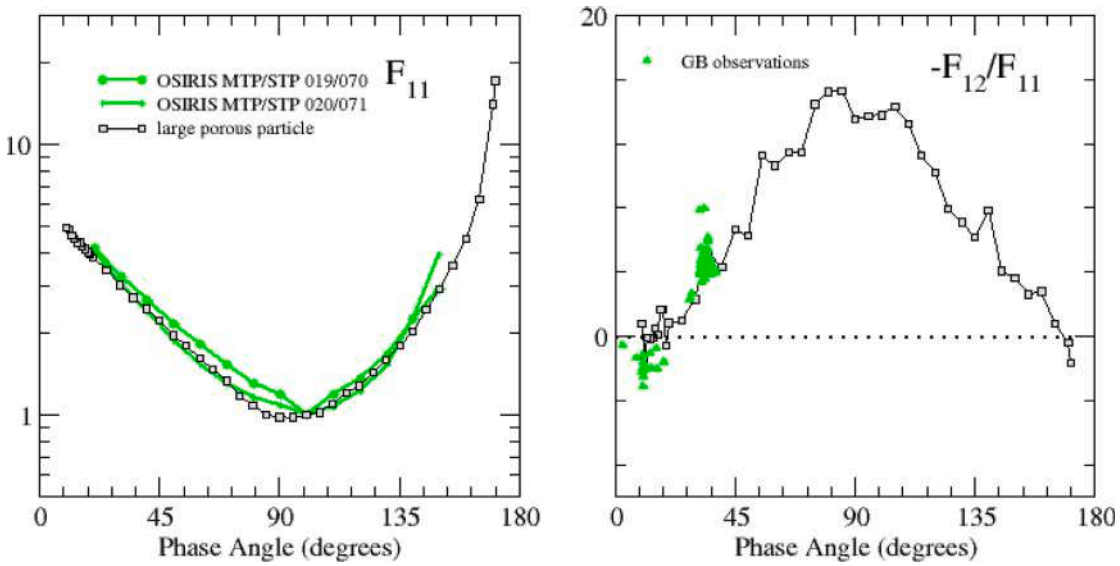

Fig. 9. Right panel: Green circles correspond to two observe phase functions from the OSIRIS camera system from [52]. Left panel: Green triangles correspond to ground-based observations of the degree of linear polarization curve for comet 67P/Churyumov–Gerasimenko ([53] and references therein). In both panels black squares correspond to experimental data for a large porous cotton ball with organic inclusions [23]. Both, phase functions a polarization curves are presented as functions of the phase angle, $\alpha = 180°\text{-}\theta$.
Source: Figure adapted from [23].

matrices for a large number of samples consisting of clouds of micron-sized particles (terrestrial aerosols, micron-sized cosmic dust analogues, meteorites and Martian dust analogs categories).

6. Applications

The data collected at GALSD can serve as a standard to validate numerical techniques aimed at reproducing the scattering patterns of irregular particles [11,16,54–60] or as input for machine learning tools [61,62]. Additionally, these data can be used to interpret observations of astronomical dusty objects, such as comets [63–65], asteroids like Bennu, the target of the Osiris Rex mission [66–68], planetary atmospheres [69,70], and protoplanetary disks [71,72].

An illustrative example on the potential use of the data in the database is related to comet 67P/Churyumov–Gerasimenko, the target of the European Space Agency's Rosetta mission. The variations in the brightness of cometary coma, as observed from Earth, depend not only on the phase angle but also on changes in the dust production rate as the comet orbits the Sun. The OSIRIS camera system aboard the Rosetta mission has provided unique observations of the light scattered by dust within the 67P coma [52]. These observations cover an unprecedentedly broad range of phase angles (from 10° to 155°). The OSIRIS dataset includes observations at various heliocentric and nucleocentric distances. In all cases, the observed phase functions exhibit a distinctive U-shape with a minimum at a phase angle of around 100°. As displayed in Fig. 9, left panel, we successfully reproduced the observational data by assuming a large porous low absorbing particle with organic inclusions. Further, the experimental-based cometary dust model can also reproduce ground-based degree of linear polarization observations of comet 67P (Fig. 9, right panel). This conclusion is in agreement with experimental data from the PROGRA2 experiment [73] and computations [74,75].

CRediT authorship contribution statement

O. Muñoz: Writing – review & editing, Writing – original draft, Supervision, Funding acquisition, Conceptualization. **E. Frattin:** Writing – review & editing, Funding acquisition. **J. Martikainen:** Software, Investigation, Formal analysis. **D. Guirado:** Software, Conceptualization. **M. Passas-Varo:** Writing – review & editing, Software, Conceptualization. **J. Escobar-Cerezo:** Software, Formal analysis, Data curation. **F.J. García-Izquierdo:** Data curation. **J.C. Gómez-Martín:** Validation, Investigation, Formal analysis. **Z. Gray:** Validation, Investigation, Data curation. **T. Jardiel:** Writing – review & editing,

Formal analysis, Data curation. **F. Moreno:** Writing – review & editing, Software, Investigation, Formal analysis. **A.J. Ocaña:** Writing – review & editing, Data curation. **M. Peiteado:** Writing – review & editing, Data curation. **A.T. Gallego-Calvente:** Software, Methodology, Conceptualization. **H. Volten:** Writing – review & editing, Methodology, Investigation, Formal analysis, Data curation, Conceptualization.

Declaration of competing interest

The authors declare that they have no known competing financial interests or personal relationships that could have appeared to influence the work reported in this paper.

Acknowledgments

This work is dedicated to the memory of Professor Joop W. Hovenier. Over 20 years ago, Joop was already aware of the need for measured light scattering data and open science. As with many other topics, he was an inspiration to many and often ahead of his time. This database would not have existed without Joop's support and innovative vision for science. This work has been funded by grant PID2021-123370OB-I00 (CATS) funded by MCIN/AEI/10.13039/501100011033, and the European Union NextGenerationEU/PTR and Severo Ochoa grant CEX2021-001131-S funded by MCIN/AEI/10.13039/501100011033.

Data availability

Data in this database are freely available under the request of citation of this paper and the paper in which the data were published.

References

[1] Volten H, de Haan JF, Hovenier JW, Schreurs R, Vassen W, Dekker AG, et al. Laboratory measurements of angular distributions of light scattered by phytoplankton and silt. Limnol Oceanogr 1998;43:1180–97. http://dx.doi.org/10.4319/lo.1998.43.6.1180.

[2] Petzold TJ. Volume scattering functions for selected ocean waters. UC San Diego: Scripps Institution of Oceanography; 1972.

[3] Volten H, Muñoz O, Hovenier JW, de Haan JF, Vassen W, van der Zande WJ, et al. WWW scattering matrix database for small mineral particles at 441.6 and 632.8nm. J Quant Spectrosc Radiat Transf 2005;90:191–206. http://dx.doi.org/10.1016/j.jqsrt.2004.03.011.

[4] Herman M, Deuzé JL, Marchand A, Roger B, Lallart P. Aerosol remote sensing from POLDER/ADEOS over the ocean: Improved retrieval using a nonspherical particle model. J Geophys Res 2005;110(D10):D10S02. http://dx.doi.org/10.1029/2004JD004798.

[5] Kahnert M, Nousiainen T, Veihelmann B. Spherical and spheroidal model particles as an error source in aerosol climate forcing and radiance computations: A case study for feldspar aerosols. J Geophys Res 2005;110(D18):D18S13. http://dx.doi.org/10.1029/2004JD005558.

[6] Moreno F, Vilaplana R, Muñoz O, Molina A, Guirado D. The scattering matrix for size distributions of irregular particles: An application to an olivine sample. J Quant Spectrosc Radiat Transf 2006;100(1–3):277–87. http://dx.doi.org/10.1016/j.jqsrt.2005.11.069.

[7] Dubovik O, Sinyuk A, Lapyonok T, Holben B, Mishchenko M, Yang P, et al. Application of spheroid models to account for aerosol particle nonsphericity in remote sensing of desert dust. J Geophys Res 2006;111(D11):D11208. http://dx.doi.org/10.1029/2005JD006619.

[8] Kahnert M, Nousiainen T. Variational data-analysis method for combining laboratory-measured light-scattering phase functions and forward-scattering computations. J Quant Spectrosc Radiat Transf 2007;103(1):27–42. http://dx.doi.org/10.1016/j.jqsrt.2006.07.011.

[9] Tyynelä J, Zubko E, Videen G, Muinonen K. Interrelating angular scattering characteristics to internal electric fields for wavelength-scale spherical particles. J Quant Spectrosc Radiat Transf 2007;106(1–3):520–34. http://dx.doi.org/10.1016/j.jqsrt.2007.01.032.

[10] Yang P, Feng Q, Hong G, Kattawar GW, Wiscombe W, Mishchenko MI, et al. Modelling of the scattering and radiative properties of nonspherical dust-like aerosols. J Aerosol Sci 2007;38(10):995–1014. http://dx.doi.org/10.1016/j.jaerosci.2007.07.001.

[11] Muinonen K, Nousiainen T, Lindqvist H, Muñoz O, Videen G. Light scattering by Gaussian particles with internal inclusions and roughened surfaces using ray optics. J Quant Spectrosc Radiat Transf 2009;110:1628–39.

[12] Volten H, Muñoz O, Hovenier JW, Waters LBFM. An update of the Amsterdam Light Scattering Database. J Quant Spectrosc Radiat Transf 2006;100(1–3):437–43. http://dx.doi.org/10.1016/j.jqsrt.2005.11.055.

[13] Muñoz O, Moreno F, Guirado D, Ramos JL, López A, Girela F, et al. Experimental determination of scattering matrices of dust particles at visible wavelengths: The IAA light scattering apparatus. J Quant Spectrosc Radiat Transf 2010;111(1):187–96. http://dx.doi.org/10.1016/j.jqsrt.2009.06.011.

[14] Muñoz O, Moreno F, Guirado D, Ramos JL, Volten H, Hovenier JW. The IAA cosmic dust laboratory: Experimental scattering matrices of clay particles. Icarus 2011;211(1):894–900. http://dx.doi.org/10.1016/j.icarus.2010.10.027.

[15] Muñoz O, Moreno F, Guirado D, Dabrowska DD, Volten H, Hovenier JW. The amsterdam-granada light scattering database. J Quant Spectrosc Radiat Transf 2012;113(7):565–74. http://dx.doi.org/10.1016/j.jqsrt.2012.01.014.

[16] Goswami B, Das HS. A study of the correlation between polarization maximum to minimum ratio and scattering parameters in a spheroid dust model. J Quant Spectrosc Radiat Transf 2023;309:108689. http://dx.doi.org/10.1016/j.jqsrt.2023.108689.

[17] Bian Y, Zhao C. Enhancing our vision of aerosols: Progress in scattering phase function measurements. Curr Pollut Rep 2024;10(1):87–104. http://dx.doi.org/10.1007/s40726-024-00292-z.

[18] Castellanos P, Colarco P, Espinosa WR, Guzewich SD, Levy RC, Miller RL, et al. Mineral dust optical properties for remote sensing and global modeling: A review. Remote Sens Environ 2024;303:113982. http://dx.doi.org/10.1016/j.rse.2023.113982.

[19] Kiselev N, Rosenbush V, Leppälä A, Muinonen K, Kolokolova L, Savushkin A, et al. New polarimetric data for the galilean satellites: Io and ganymede observations and modeling. Planet Sci J 2024;5(1):10. http://dx.doi.org/10.3847/PSJ/ad0bf9.

[20] Zubko E, Zheltobryukhov M, Chornaya E, Shmirko KA, Lisitsa VV, Pavlov AN, et al. Characterizing atmospheric aerosols using polarimetry and shadow hiding. Front Remote Sens 2024;4:1321621. http://dx.doi.org/10.3389/frsen.2023.1321621.

[21] Hovenier JW. Measuring scattering matrices of small particles at optical wavelengths. In: Light scattering by nonspherical particles: theory, measurements, and applications. 2000, p. 355.

[22] Hovenier JW, Volten H, Munoz O, van der Zande WJ, Waters LB. Laboratory study of scattering matrices for randomly oriented particles: Potentials, problems, and perspectives. J Quant Spectrosc Radiat Transf 2003;79–80:741. http://dx.doi.org/10.1016/S0022-4073(02)00319-9.

[23] Muñoz O, Moreno F, Gómez-Martín JC, Vargas-Martín F, Guirado D, Ramos JL, et al. Experimental phase function and degree of linear polarization curves of millimeter-sized cosmic dust analogs. Astrophys J Suppl 2020;247(1):19. http://dx.doi.org/10.3847/1538-4365/ab6851.

[24] Hansen JE, Travis LD. Light scattering in planetary atmospheres. Space Sci Rev 1974;16(4):527–610. http://dx.doi.org/10.1007/BF00168069.

[25] Hovenier JW. Measuring scattering matrices of small particles at optical wavelengths. In: Mishchenko MI, Hovenier JW, Travis LD, editors. Light scattering by nonspherical particles : theory, measurements, and applications. 2000.

[26] Volten H, Muñoz O, Rol E, de Haan JF, Vassen W, Hovenier JW, et al. Scattering matrices of mineral aerosol particles at 441.6 nm and 632.8 nm. J Geophys Res 2001;106(D15):17375–402. http://dx.doi.org/10.1029/2001JD900068.

[27] Muñoz O, Moreno F, Vargas-Martín F, Guirado D, Escobar-Cerezo J, Min M, et al. Experimental phase functions of millimeter-sized cosmic dust grains. Astrophys J 2017;846(1):85. http://dx.doi.org/10.3847/1538-4357/aa7ff2, arXiv:1707.04158.

[28] Ren BB, Benisty M, Ginski C, Tazaki R, Wallack NL, Milli J, et al. Protoplanetary disks in K_s-band total intensity and polarized light. Astron Astrophys 2023;680:A114. http://dx.doi.org/10.1051/0004-6361/202347353, arXiv:2310.08589.

[29] Güttler C, Mannel T, Rotundi A, Merouane S, Fulle M, Bockelée-Morvan D, et al. Synthesis of the morphological description of cometary dust at comet 67P/Churyumov-Gerasimenko. Astron Astrophys 2019;630:A24. http://dx.doi.org/10.1051/0004-6361/201834751, arXiv:1902.10634.

[30] Gray Z, Bagnulo S, Granvik M, Cellino A, Jones GH, Kolokolova L, et al. Polarimetry of didymos–dimorphos: Unexpected long-term effects of the DART impact. Planet Sci J 2024;5(1):18. http://dx.doi.org/10.3847/PSJ/ad0f18, arXiv:2311.13483.

[31] Muñoz O, Volten H, de Haan JF, Vassen W, Hovenier JW. Experimental determination of the phase function and degree of linear polarization of El Chichón and Pinatubo volcanic ashes. J Geophys Res (Atmospheres) 2002;107(D13):4174. http://dx.doi.org/10.1029/2001JD000983.

[32] Muñoz O, Volten H, Hovenier JW, Veihelmann B, van der Zande WJ, Waters LBFM, et al. Scattering matrices of volcanic ash particles of Mount St. Helens, Redoubt, and Mount Spurr Volcanoes. J Geophys Res (Atmospheres) 2004;109(D16):D16201. http://dx.doi.org/10.1029/2004JD004684.

[33] Gómez Martín JC, Guirado D, Frattin E, Bermudez-Edo M, Cariñanos Gonzalez P, Olmo Reyes FJ, et al. On the application of scattering matrix measurements to detection and identification of major types of airborne aerosol particles: Volcanic ash, desert dust and pollen. J Quant Spectrosc Radiat Transf 2021;271:107761. http://dx.doi.org/10.1016/j.jqsrt.2021.107761.

[34] Muñoz O, Frattin E, Jardiel T, Gómez-Martín JC, Moreno F, Ramos JL, et al. Retrieving dust grain sizes from photopolarimetry: An experimental approach. Astrophys J Suppl 2021;256(1):17. http://dx.doi.org/10.3847/1538-4365/ac0efa, arXiv:2109.05764.

[35] Veihelmann B, Volten H, van der Zande WJ. Light reflected by an atmosphere containing irregular mineral dust aerosol. Geophys Res Lett 2004;31(4):L04113. http://dx.doi.org/10.1029/2003GL018229.

[36] Martín JG, Guirado D, Zubko E, Escobar-Cerezo J, Moreno F, Muñoz O. Computational study of the sensitivity of laser light scattering particle sizing to refractive index and irregularity. J Quant Spectrosc Radiat Transf 2020;241:106745. http://dx.doi.org/10.1016/j.jqsrt.2019.106745.

[37] Martikainen J, Penttilä A, Gritsevich M, Lindqvist H, Muinonen K. Spectral modeling of meteorites at UV-vis-NIR wavelengths. J Quant Spectrosc Radiat Transf 2018;204:144–51. http://dx.doi.org/10.1016/j.jqsrt.2017.09.017.

[38] Martikainen J, Muñoz O, Jardiel T, Gómez Martín JC, Peiteado M, Willame Y, et al. Optical constants of martian dust analogs at UV-visible-near-infrared wavelengths. Astrophys J Suppl 2023;268(2):47. http://dx.doi.org/10.3847/1538-4365/acf0be.

[39] Mishchenko MI, Yurkin MA. On the concept of random orientation in far-field electromagnetic scattering by nonspherical particles. Opt Lett 2017;42(3):494. http://dx.doi.org/10.1364/OL.42.000494.

[40] Renard J-B, Geffrin J-M, Valencia VT, Tortel H, Ménard F, Rannou P, et al. Number of independent measurements required to obtain reliable mean scattering properties of irregular particles having a small size parameter, using microwave analogy measurements. J Quant Spectrosc Radiat Transf 2021;272:107718. http://dx.doi.org/10.1016/j.jqsrt.2021.107718.

[41] Vaillon R, Geffrin J-M, Eyraud C, Merchiers O, Sabouroux P, Lacroix B. A new implementation of a microwave analog to light scattering measurement device. J Quant Spectrosc Radiat Transf 2011;112:1753–60. http://dx.doi.org/10.1016/j.jqsrt.2010.12.008.

[42] Colin A, Muñoz O, García-Izquierdo F, Frattin E, Martikainen J, Guirado D, et al. An acoustic levitator design for suspending cosmic dust analogues and aerosol particles in light scattering experiments. 2024, In preparation.

[43] Muñoz O, Volten H, de Haan JF, Vassen W, Hovenier JW. Experimental determination of scattering matrices of olivine and Allende meteorite particles. Astron Astrophys 2000;360:777–88.

[44] Volten H, Muñoz O, Brucato JR, Hovenier JW, Colangeli L, Waters LBFM, et al. Scattering matrices and reflectance spectra of forsterite particles with different size distributions. J Quant Spectrosc Radiat Transf 2006;100(1–3):429–36. http://dx.doi.org/10.1016/j.jqsrt.2005.11.074.

[45] Martikainen J, Muñoz O, Gómez Martín J, Jardiel T, Peiteado M, Caballero A, et al. Experimental scattering matrices of martian dust aerosols with narrow particle-size distributions. Astrophys J Suppl 2024;273(2):28. http://dx.doi.org/10.3847/1538-4365/ad5720.

[46] Lindqvist H, Muinonen K, Nousiainen T. Light scattering by coated Gaussian and aggregate particles. J Quant Spectrosc Radiat Transf 2009;110:1398–410.

[47] Lindqvist H, Nousiainen T, Zubko E, Muñoz O. Optical modeling of vesicular volcanic ash particles. J Quant Spectrosc Radiat Transf 2011;112:1871–80. http://dx.doi.org/10.1016/j.jqsrt.2011.01.032.

[48] Moreno F, Muñoz O, López-Moreno JJ, Molina A, Ortiz JL. A Monte Carlo code to compute energy fluxes in cometary nuclei. Icarus 2002;156(2):474–84. http://dx.doi.org/10.1006/icar.2001.6806.

[49] Hovenier JW, Guirado D. Zero slopes of the scattering function and scattering matrix for strict forward and backward scattering by mirror symmetric collections of randomly oriented particles. J Quant Spectrosc Radiat Transf 2014;133:596–602. http://dx.doi.org/10.1016/j.jqsrt.2013.09.023.

[50] Escobar-Cerezo J, Muñoz O, Moreno F, Guirado D, Gómez Martín JC, Goguen JD, et al. An experimental scattering matrix for lunar regolith simulant JSC-1A at visible wavelengths. Astrophys J Suppl 2018;235(1):19. http://dx.doi.org/10.3847/1538-4365/aaa6cc.

[51] Guirado D, Muñoz O. Chapter 13 - particle characterization with laboratory nephelometers. In: Mengüç MP, Francoeur M, editors. Light, plasmonics and particles. Nanophotonics, Elsevier; 2023, p. 271–93. http://dx.doi.org/10.1016/B978-0-323-99901-4.00007-X, URL https://www.sciencedirect.com/science/article/pii/B978032399901400007X.

[52] Bertini I, La Forgia F, Tubiana C, Güttler C, Fulle M, Moreno F, et al. The scattering phase function of comet 67P/Churyumov-Gerasimenko coma as seen from the Rosetta/OSIRIS instrument. Mon Not R Astron Soc 2017;469:S404–15. http://dx.doi.org/10.1093/mnras/stx1850.

[53] Rosenbush VK, Ivanova OV, Kiselev NN, Kolokolova LO, Afanasiev VL. Spatial variations of brightness, colour and polarization of dust in comet 67P/Churyumov-Gerasimenko. Mon Not R Astron Soc 2017;469:S475–91. http://dx.doi.org/10.1093/mnras/stx2003.

[54] Nousiainen T, Vermeulen K. Comparison of measured single-scattering matrix of feldspar with T-matrix simulations using spheroids. J Quant Spectrosc Radiat Transf 2003;79–80:1031. http://dx.doi.org/10.1016/S0022-4073(02)00337-0.

[55] Min M, Hovenier JW, de Koter A. Modeling optical properties of cosmic dust grains using a distribution of hollow spheres. Astron Astrophys 2005;432(3):909–20. http://dx.doi.org/10.1051/0004-6361:20041920, arXiv:astro-ph/0503068.

[56] Merikallio S, Lindqvist H, Nousiainen T, Kahnert M. Modelling light scattering by mineral dust using spheroids: assessment of applicability. Atmos Chem Phys 2011;11(11):5347–63. http://dx.doi.org/10.5194/acp-11-5347-2011.

[57] Lindqvist H, Jokinen O, Kandler K, Scheuvens D, Nousiainen T. Single scattering by realistic, inhomogeneous mineral dust particles with stereogrammetric shapes. Atmos Chem Phys 2014;14(1):143–57. http://dx.doi.org/10.5194/acp-14-143-2014.

[58] Saito M, Yang P, Ding J, Liu X. A comprehensive database of the optical properties of irregular aerosol particles for radiative transfer simulations. J Atmos Sci 2021;78(7):2089–111. http://dx.doi.org/10.1175/JAS-D-20-0338.1.

[59] Lin W, Bi L, Weng F, Li Z, Dubovik O. Capability of superspheroids for modeling PARASOL observations under dusty-sky conditions. J Geophys Res 2021;126(1). http://dx.doi.org/10.1029/2020JD033310, e2020JD033310.

[60] Huang Y, Kok JF, Saito M, Muñoz O. Single-scattering properties of ellipsoidal dust aerosols constrained by measured dust shape distributions. Atmos Chem Phys 2023;23(4):2557–77. http://dx.doi.org/10.5194/acp-23-2557-2023.

[61] Piedra P, Kalume A, Zubko E, Mackowski D, Pan Y-L, Videen G. Particle-shape classification using light scattering: An exercise in deep learning. J Quant Spectrosc Radiat Transf 2019;231:140–56. http://dx.doi.org/10.1016/j.jqsrt.2019.04.013.

[62] Moon CY, Gargiulo A, Byun G, Todd Lowe K. Non-spherical particle size estimation using supervised machine learning. Appl Opt 2020;59(10):3237. http://dx.doi.org/10.1364/AO.385750.

[63] Frattin E, Muñoz O, Moreno F, Nava J, Escobar-Cerezo J, Gomez Martin JC, et al. Experimental phase function and degree of linear polarization of cometary dust analogues. Mon Not R Astron Soc 2019;484(2):2198–211. http://dx.doi.org/10.1093/mnras/stz129, arXiv:1901.05975.

[64] Kochergin A, Zubko E, Chornaya E, Zheltobryukhov M, Videen G, Kornienko G, et al. Monitoring the negative polarization in Comet 29P/Schwassmann-Wachmann during quiescence. Icarus 2021;366:114536. http://dx.doi.org/10.1016/j.icarus.2021.114536.

[65] Voitko A, Zubko E, Ivanova O, Luk'yanyk I, Kochergin A, Husárik M, et al. Color variations of comet 29P/Schwassmann-Wachmann 1 in 2018. Icarus 2022;388:115236. http://dx.doi.org/10.1016/j.icarus.2022.115236.

[66] Hergenrother CW, Maleszewski C, Li JY, Pajola M, Chesley SR, French AS, et al. Photometry of particles ejected from active asteroid (101955) bennu. J Geophys Res (Planets) 2020;125(9):e06381. http://dx.doi.org/10.1029/2020JE006381.

[67] Frattin E, Martikainen J, Muñoz O, Gómez-Martín JC, Jardiel T, Cellino A, et al. Experimental phase function and degree of linear polarization curve of olivine and spinel and the origin of the Barbarian polarization behaviour. Mon Not R Astron Soc 2022;517(4):5463–72. http://dx.doi.org/10.1093/mnras/stac2895.

[68] Lolachi R, Glenar DA, Stubbs TJ, Kolokolova L. Optical characterization of the DART impact plume: Importance of realistic ejecta scattering properties. Planet Sci J 2023;4(2):24. http://dx.doi.org/10.3847/PSJ/aca968.

[69] Mishchenko M, Geogdzhaev I, Liu L, Orgen A, Lacis A, Rossow W, et al. Aerosol retrievals from AVHRR radiances: effects of particle nonsphericity and absorption and an updated long-term global climatology of aerosol properties. J Quant Spectrosc Radiat Transf 2003;79–80:953. http://dx.doi.org/10.1016/S0022-4073(02)00331-X.

[70] Chen-Chen H, Pérez-Hoyos S, Sánchez-Lavega A. Characterisation of Martian dust aerosol phase function from sky radiance measurements by MSL engineering cameras. Icarus 2019;330:16–29. http://dx.doi.org/10.1016/j.icarus.2019.04.004, arXiv:1905.01074.

[71] Ren B, Choquet E, Perrin MD, Duchêne G, Debes JH, Pueyo L, et al. An exo-kuiper belt with an extended halo around HD 191089 in scattered light. Astrophys J 2019;882(1):64. http://dx.doi.org/10.3847/1538-4357/ab3403, arXiv:1908.00006.

[72] Lin Z-YD, Li Z-Y, Yang H, Muñoz O, Looney L, Stephens I, et al. (Sub)millimetre dust polarization of protoplanetary discs from scattering by large millimetre-sized irregular grains. Mon Not R Astron Soc 2023;520(1):1210–23. http://dx.doi.org/10.1093/mnras/stad173, arXiv:2206.12357.

[73] Levasseur-Regourd AC, Renard JB, Hadamcik E, Lasue J, Bertini I, Fulle M. Interpretation through experimental simulations of phase functions revealed by Rosetta in 67P/Churyumov-Gerasimenko dust coma. Astron Astrophys 2019;630:A20. http://dx.doi.org/10.1051/0004-6361/201834894, arXiv:1905.12508.

[74] Markkanen J, Agarwal J, Väisänen T, Penttilä A, Muinonen K. Interpretation of the phase functions measured by the OSIRIS instrument for comet 67P/Churyumov-Gerasimenko. Astrophys J Lett 2018;868(1):L16. http://dx.doi.org/10.3847/2041-8213/aaee10, arXiv:1811.03899.

[75] Moreno F, Guirado D, Muñoz O, Bertini I, Tubiana C, Güttler C, et al. Models of rosetta/OSIRIS 67P dust coma phase function. Astron J 2018;156(5):237. http://dx.doi.org/10.3847/1538-3881/aae526, arXiv:1809.10424.